Laser ablation of metal into liquid: Near critical point phenomena and hydrodynamic instability

Nail Inogamov, Vasily Zhakhovsky, and Viktor Khokhlov

Citation: AIP Conference Proceedings **1979**, 190001 (2018); doi: 10.1063/1.5045043
View online: https://doi.org/10.1063/1.5045043
View Table of Contents: http://aip.scitation.org/toc/apc/1979/1
Published by the American Institute of Physics

Laser Ablation of Metal into Liquid: near Critical Point Phenomena and Hydrodynamic Instability

Nail Inogamov[1,2,a)], Vasily Zhakhovsky[2,1] and Viktor Khokhlov[1]

[1]*Landau Institute for Theoretical Physics, Chernogolovka 142432, Russia*
[2]*Dukhov Research Institute of Automatics, Moscow 127055, Russia*

[a)]Corresponding author: nailinogamov@gmail.com

Abstract. We consider the problem of dynamics of gold illuminated through water by ultrashort laser pulse. This problem is interesting itself due to its complexity and it is important for nanotechnological applications connected with a clean way (without chemistry) of nanoparticles production and also for creation of functional surfaces (e.g. for enhancing of surface Raman scattering) which differ from the functional surfaces produced by illumination through vacuum or gas. We begin with short presentation of the two-temperature phenomena inevitable when the ultrashort laser pulse is used. We present results of two-temperature (2T) one-dimensional hydrodynamic (2T-HD) simulations covering very long (up to 0.2μsec) time interval. This is significant because namely at these late times pressure at a contact boundary between gold (Au) and glass decreases down to saturation pressure of gold. And the saturation pressure begins to influence dynamics near the contact. Inertia of water is the next main actor. It decelerates the contact. In the reference frame connected with the contact the deceleration is equivalent to the free fall acceleration in a gravity field. This follows from the Einstein's principle of the gravity/inertia equivalence. This is exact the conditions favorable for development of Rayleigh-Taylor (RT) instability (RTI) because heavy fluid (Au) is placed above the light one (water) in a gravity field. We extract the increment of RTI from 2T-HD 1D runs. Surface tension and especially viscosity significantly dump the RTI gain during deceleration. We use large scale molecular dynamics (MD) simulations to do the situation clear. MD runs show that significant amplification of surface perturbations takes place. These perturbations start just from thermal fluctuations and the noise produced by bombardment of the atmosphere by fragments of foam. The perturbations achieve amplification enough to separate the droplets from the RTI jets of gold. Thus the droplets fall into water. There is a quasi-hydrostatic equilibrium near the contact in gold. Therefore we use the word "atmosphere". Laser action should be strong to produce nanoparticles. It is significantly higher than the nucleation threshold F_{abl} for gold thermo-mechanically ablated into vacuum. Absorbed energy F_{abs} is of the order of or higher than the evaporation (ev) threshold $F_{abs}|_{ev}$ above which the spallation plate cannot form during expansion of gold to vacuum. In this case very wide foamy zone is created. Expansion of foam doesn't "know" about water. Foam expands freely. Thus its expansion velocities begin overcome velocity of a contact decelerated by water. This causes accretion of membranes of foam onto atmosphere created thanks to deceleration. The MD simulations beautifully illustrate this flow with shock in water, atmosphere "sitting on water", vast foam, RTI of the contact, and accretion of foam onto atmosphere.

INTRODUCTION

Laser ablation of metal in contact with liquid differs much from ablation into vacuum. In spite of importance of this type of laser-matter interaction (e.g., for nanoparticles production), the involved processes are still poorly understood. But a lot of experimental works were already performed – see the recent extensive review in [1].

We show that to produce nanoparticles the laser absorbed energy F_{abs} should exceed the ablation threshold $F_{abs}|_{abl}$ into vacuum by a few times; $F_{abs}|_{abl} \approx 100\,\mathrm{mJ/cm^2}$ for gold [2, 3]. Here the ablation with $F_{abs} = 400\,\mathrm{mJ/cm^2}$ is studied. As a result of large energy absorbed in gold the temperatures in the heat-affected zone (HAZ) increase above the critical temperature. The flow of the substances, including propagation of a strong shock in liquid and a rarefaction wave inside the metal target, is analyzed. We demonstrate that the contact between metal and liquid, both being in their supercritical states, is unstable, which leads to the Rayleigh-Taylor instability. Dynamics of the instability is important for separation of melt droplets, which are frozen to solid nanoparticles later.

There are a chain in time of interrelated physical phenomena. Processes begin with absorption of ultrashort pulse (durations $\sim 0.1 - 1$ps) and two-temperature (2T) stage $T_e \gg T_i$ covering duration of a pulse and finishing when electron T_e and ion T_i temperatures equalize. Our approach for this stage was described earlier [4, 5] therefore we

Shock Compression of Condensed Matter - 2017
AIP Conf. Proc. 1979, 190001-1–190001-6; https://doi.org/10.1063/1.5045043
Published by AIP Publishing. 978-0-7354-1693-2/$30.00

omit its description in this short paper. The heat-affected zone (HAZ) is formed during the 2T stage. Its thickness for gold is $d_T \approx 150$nm. The HAZ is formed inside gold independently of presence or absence of water.

The chain of processes proceeds with acoustic decay of HAZ, see Section 2. In the case of high F_{abs} considered here, vast region occupied by foam is formed as a result of decay of HAZ. Foam is a mixture of liquid and vapor phases with low volume content of liquid in a unit volume of mixture. Foam develops during expansion of zone of nucleations. Acoustic impedance z_{wt} of water is small relative to that for gold $z_{Au}/z_{wt} \approx 7$. Therefore presence of water is an insignificant factor at the stage of decay of liquid condensed Au into two-phase mixture; this stage is studied in Section 2; the stage lasts during an acoustic time scale $t_s = d_T/c_s$, where c_s is speed of sound. But later in time the main part of foam accretes onto atmosphere appearing namely due to presence of water.

DECAY OF METAL INTO VACUUM OR LIQUID

There are two type of experiments with different lateral size of an irradiated spot (radius R_L) at a surface. People use diffraction limited tight focusing when $R_L \sim \lambda$ in the first type of experiments; for optical lasers $\lambda \sim 1\mu$m. While in the other type the large spots (R_L is many microns) are necessary. For massive nanoparticle production and for creation of functional surfaces the large spots are used. Functional surfaces are covered by random nanostructures.

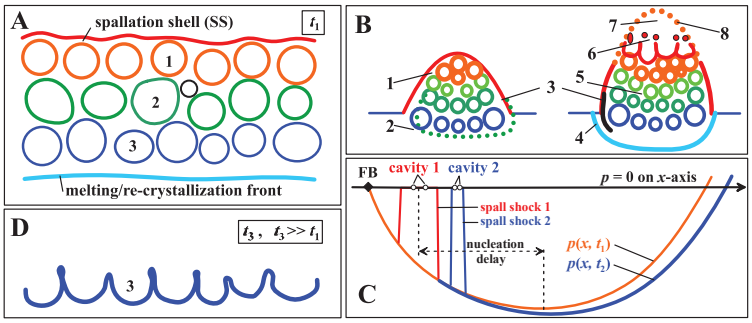

FIGURE 1. A. Melting front, foam, and SS. **B.** Systems of finite lateral sizes R_L are shown; the frames A and D correspond to the radius $R_L = \infty$. The systems in frame B consist from cupola SS "1" which is closed if $F_{abs}|_{abl} < F_{abs} < F_{abs}|_{ev}$ and open in central region "7, 8" if $F_{abs}|_{ev} < F_{abs}$. **C.** Nucleation for fluences greatly above the ablation threshold. This is the main case considered below. This is a start stage for processes producing the reach multilayered foam shown in frames A and B, which then finish with the structured surface in frame D. This regime is favorable to production of nanoparticles in vacuum or liquid.

For large spots the surface tension defines spatial scales of frozen random structures placed at the bottom of a crater (see Figure 1D) and observed in experiments after a single or few shots action; many peoples saw them [6–10] and have advanced useful applications of these structured surfaces for changing optical [6], mechanical (strength, tribology, wettability), These capillary scales are much smaller than diameter of a large crater [8, 10]. They form during expansion and breaking of a liquid-vapor foam, see Figures 1C (appearance of nuclei), 1A (development and expansion of nuclei), 1D (final state formed after breaking and freezing), and [10]. Significantly above ablation threshold a deep foam layer appears. This is illustrated in Figure 1A by the bubble layers "1-2-3" in the foam. Nucleation of the layer "1" proceeds first. How the first nuclei appears and how they influence rarefaction is shown in Figure 1C and in Figure 2 below. There is a spallation shell above the bubble layers in the case $F_{abs}|_{abl} < F_{abs} < F_{abs}|_{ev}$.

Above the "evaporation" (ev) threshold $F_{abs}|_{ev}$ the integral shell SS covering the foam in Figure 1A disappears. Bubbles develop in molten metal, therefore at the early stages the melting front in Figure 1A is below the foam. Later in time the shell and membranes in the upper bubble layers break off and fly away. The remnants of the layer "3" in Figure 1D remain and solidify at the bottom of a crater "2" shown in Figure 1B. These remnants form the random relief in Figure 1D. In Figure 1B the bottom of the crater remaining at the surface is "2", this bottom is shown in frame D. The ring structure around the crater is "3" in Figure 1B. Melting/re-solidification front is "4". The bubble interior is "5". The "6" in Figure 1B is a vapor-droplet zone ahead the closed bubbles separated from each other by membranes. With rupture of membranes the bubble zone gradually transforms to the vapor-droplet zone.

Ring shape around a crater appears in competition between capillarity and re-solidification, see Figure 1B where it is marked by "3". The ring corresponds to a region near the thermomechanical threshold where (around the ring) small open and closed undersurface bubbles locate [11, 12]. Development of a crater may be imaged as inflation of a large bubble together with inflation of foam filling this bubble, and successive ruptures of membranes forming foam beginning from the upper layers of bubbles, see Figures 1A, 1D and 1B.

Capillary velocities v_σ are rather low, usually ~10 m/s. But surface tension phenomena, e.g. the final crater nanostructures, aren't excluded if laser action is strong and expansion velocities are higher than v_σ; they are not

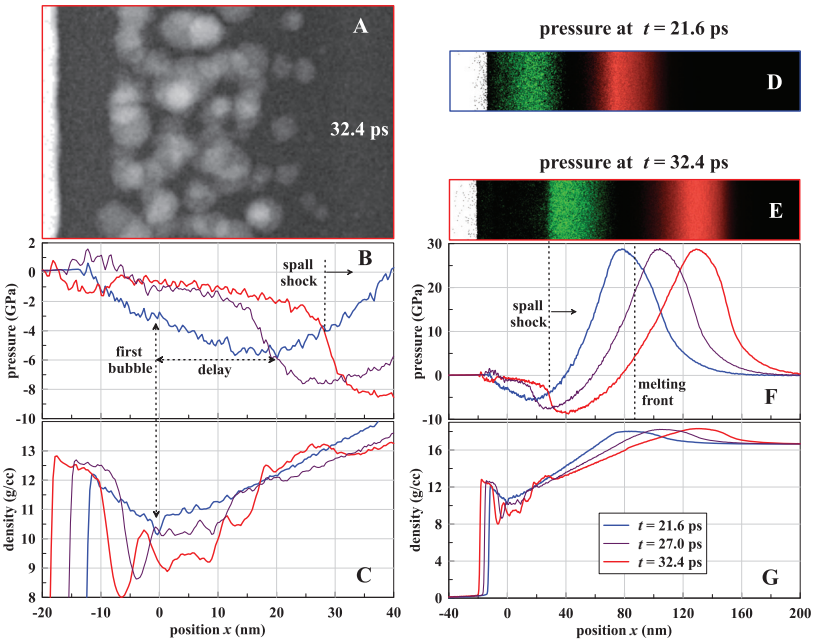

FIGURE 2. Simulation of ultrashort laser action onto tantalum sample with dimensions $400.1 \times 40.2 \times 20.1$ nm^3, number of atoms 17.9×10^6, HAZ 40 nm (Gaussian distribution), $F_{abs} = 275$ mJ/cm^2. **A.** The map of density integrated along the ray perpendicular to the plane of picture. We see the ensemble of the 3D cavities; neither of them forms through hole (through thickness of simulation box in direction perpendicular to the plane of picture), therefore 3D. **F.** The pressure profiles in whole. They are repeated in frames D and E as the pressure maps - the colors of those frames corresponds to the colors of the curves presenting the profiles. **D, E.** We see the compression (red color) and rarefaction waves (green) together with unloaded region with small pressures (black color) in Figure E. The right edge of the black region in Figure E relates to the spall shock. **B, F** and **C, G** are pressure and density profiles, resp.

excluded if a film is thick enough to keep a cold interior. In bulk targets a strong action (i.e. significantly, at least few times, above ablation threshold) drives a cascade of nucleations shown in Figures 1 and 2. Figures 1C and 2 illustrates how the layers of bubbles (cavities) in the cascade of layers form. There are successive nucleation "flashes" as a rarefaction wave "sitting" at the shock front penetrates into a target. The scheme of them is presented in Figure 1C.

Nucleation event produces a spherical shock expanding around cavity. The first cavities are located along a plane layer shown in Figure 1C as "cavity 1". Spherical waves interfere and form two plane spall waves propagating to the left and to the right side relative the layer of cavities. The right shock is shown as "spall shock 1" in Figure 1C. Two small circles "cavity 1" mark off the "banks" of the rupture where in the Lagrangian 1D simulation density drops to zero; an empty gap between two neighboring Lagrangian particles appears. In MD there is a well in density profile between these banks, see Figure 2B and 2C where the first well is marked by the two side arrow. The arrow shows the point of the first nucleation where density decreases, while pressure increases.

The spall shock unload tensile stress increasing pressure from negative value to the value $p = 0$ as it is shown on pressure profile $p(x, t_1)$ in Figure 1C by the two vertical straights around the "cavity 1"; the right straight is underlined by caption "spall shock 1". The "spall shock 1" propagates to the right side with speed which slightly surpasses local speed of sound c_s. The excess above c_s is proportional to a nonlinearity degree of a spall shock. Nonlinearity is weak therefore the excess is small.

Non-trivial is the regime of multiple nucleations in the successive layers. The next nucleation takes place ahead the spall shock propagating from the previous event. The "cavity 2" in Figure 1C appears to the right side relative to "spall shock 1", i.e. outside the unloading influence of the "spall shock 1". The "cavity 2" event produces its own "spall shock 2". Thus the spall shock front during multiple nucleations loses its causal relationship with "old" nucleation events. In such regime the spall shock runs with phase velocity. This velocity surpasses speed of sound but not in connection with non-linearity as in the case of a single nucleation layer.

We see that the current position of a spall shock is defined by the last nucleation layer. This is true while the nucleation zone develops into bulk matter capturing new and new masses. When nucleation ceases then the spall shock returns to its unsupported (by successive nucleations), weakly non-linear regime of propagation.

The well of $p < 0$ in the pressure profile shown in Figure 2F has two branches to the left and right sides relative to the instant minimum. As a rarefaction wave propagates to the right - the minimum and the right branch shift to the right, while the left branch remains approximately the same, only minimum becomes deeper, thus the left branch is prolonged more far down - up to the current minimum, compare the profiles $p(x, t_1)$ and $p(x, t_2 > t_1)$ in Figure 1C. This is the situation without nucleations. During this process of lowering of the minimum, the beginning of the left branch is pinned to the point "FB" in Figure 1C; FB means free surface of condensed phase bordering with vapor. At acoustic time scale $t_s = d_T/c_s$ the process of lowering of the minimum terminates; here d_T is thickness of a heat

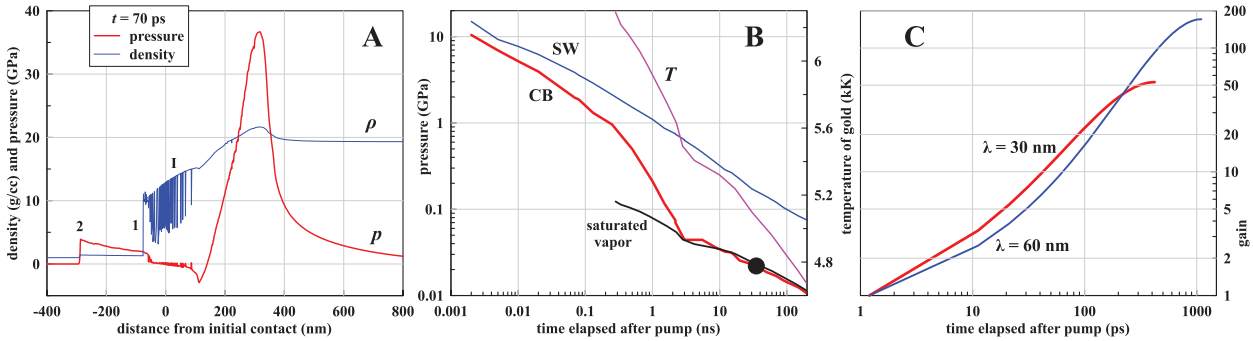

FIGURE 3. Simulation of expansion of gold into water; 2T-HD code, $F_{abs} = 400$ mJ/cm^2, **A.** Profiles of compression wave propagating to the right. The wave becomes steeper and overturns forming a shock. Cavitation zone is important for gold-water interaction. Pressure in this zone is small. This it is wide because energy is large. Small increase of density and pressure at the left end of cavitation zone corresponds to the atmosphere. It is supported by contact pressure. **B.** Decay in time of pressures at shock in water (curve "SW") and at the contact boundary "CB". Contact pressure drops down to saturation pressure in gold at temperatures of atmosphere shown by the curve "T". Further drop decreases contact pressure down to critical pressure of water (black circle). **C.** Linear gain of perturbation amplitudes calculated from known from simulation dependence of deceleration $g(t)$ and values for surface tension and viscosity of gold taken from reference books. We chose typical perturbation wavelengths 30 and 60 nm.

affected zone (HAZ); the HAZ is created during a two-temperature stage. Then the lowering finishes, the beginning of the left branch comes uncoupled with the free surface and begins to move with speed of sound into interior. Pressure at the interval connecting the free surface and the moving beginning equals to vapor pressure.

This was the situation without nucleation. At the nucleation threshold the first and last layer of cavities appears in the minimum of the pressure profile when the minimum achieves its deepest point. We are interested in the case significantly (few times and more) above the nucleation threshold. Then the first plane layer of cavities ("cavity 1" in Figure 1C) (i) nucleate at some distance "nucleation delay" behind the current position of a minimum in Figure 1C, while (ii) the minimum continues to get deeper into $p < 0$ region. It seems that this is the same minimum of the "pure" rarefaction wave unaffected (therefore it is said "pure") by the "wave" of successive nucleation events coming from the left side relative to the current minimum. At least in Figures 2B and 2F the plum and red minimums look like "sitting" at the continuation of the blue profile weakly influenced by nucleation.

In the simulation shown in Figure 2 the cascade of nucleations ceases near the instant 32ps before the instant $t_* \sim t_s$ when the minimum achieves its deepest depth. The right bubbles in Figure 2A are the last ones. In our conditions the thermo-fluctuating mechanism of nucleation works. Probability to born a nucleus is proportional to $\exp(-W/T)$, $W = (16\pi/3)\sigma^3/(T\,p^2)$, where W is work necessary to born a nucleus, $\sigma(T)$ is surface tension. Ending of nucleations is caused by decrease of temperature T with distance from the free surface as we approach the melting front shown in Figure 2F.

Spall shock transfers into its usual (unsupported by nucleations) propagation regime after finishing of appearing of new bubbles. At late stages the spall shock neutralizes the well of negative pressure because it moves slightly faster than the local acoustic characteristics of the rarefaction wave because of its non-linear propagation (slightly above the local current speed of sound).

Hydrodynamic velocities of foam expansion decrease from external (#1 in Figure 1A) to internal (#3 in Figure 1A) successive layers "1-2-3" which make the cascade [6, 10]. Foam develops from the nucleated vapor cavities as they inflate decreasing a volume part of liquid in the liquid-vapor mixture. Near the practically motionless bottom of a crater, the velocities in the bottom layer #3 in Figure 1A drops down to v_σ. This condition corresponds to the last layer where propagation of a nucleation zone into a target ceases (instant t_1, Figure 1A). Later in time, capillary remnants of this layer remain on a target, freeze, and form a final surface topology, while the spallation shell together with the upper bubble layers separate from a target and fly away (instant t_3, Figure 1D) [10].

The spallation shell isn't created above the evaporation threshold F_{ev} introduced in [2, 13]; see also classification of 3 regimes of expansion between two thresholds (ablation and evaporation) in Figure 14 [2], Figure 16 [14], and in [15]. The spallation shell isn't created because the upper layer is too hot - high temperature almost totally suppresses cohesion attraction between atoms. In the case $F > F_{ev}$ a plasma or hot vapor ejecta precedes the expanding bubble layers. The cases with and without a spallation shell are compared in Figure 1B.

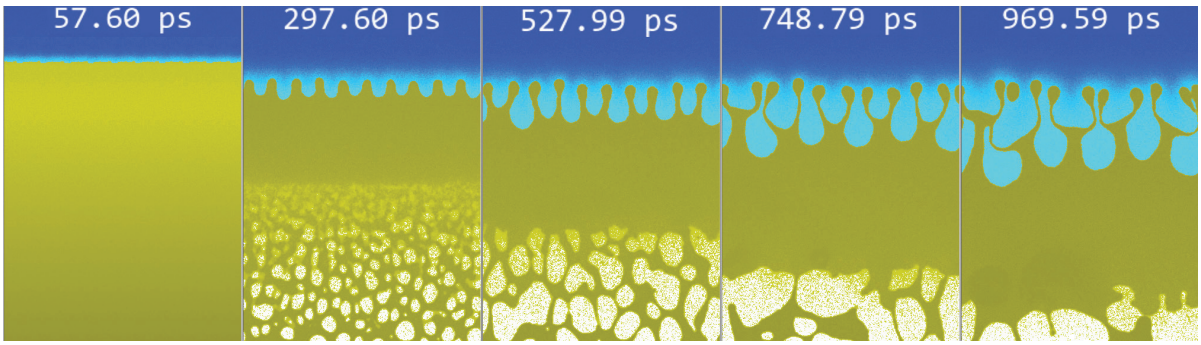

FIGURE 4. Evolution of the near contact situation; water is blue, gold is yellow. We see formation and development of foam, due to inflation the cells in foam enlarge, contact is decelerated by water, a layer of continuous gold appears at the contact, we call "atmosphere" this layer (because it is hydrostatically supported by water), atmosphere decelerates, thus it velocity decreases, while foam "doesn't know" about water and expands freely - this means with larger current velocity than atmosphere. Therefore foam accretes onto the atmosphere. Water is heated through atom-atom conduction from hot gold. Heated water has less blue color. It is located in growing bubbles near the contact. Due to deceleration of dense matter (gold) by light one (water) the contact is unstable to Rayleigh-Taylor instability (RTI). Therefore the well known structure made from bubbles and jets deforms the contact. Non-linear development of this structure causes appearance of gold droplets in water.

Evolution of cavitated fluid is shown in Figure 1A and 1D. Rarefaction wave runs with speed of sound (leaving the trace with successive nucleation layers, see Figure 1C and 2) while hydrodynamic expansion of foam proceeds slowly. Therefore bubbles in the successive layers "1-2-3" in Figure 1A differ moderately in their sizes, see also Figure 2A; although the layer "1" appears before the all successive layers in Figure 1A. At t_1 metal is molten above the melting/re-crystallization front in Figure 1A. The final surface structure solidifies before the instant t_3 in Figure 1D. This structure is a frozen trace of the last layer of bubbles. Foamy matter confined inside the spallation shell is shown in Figure 1B. In the case with hot central region $F > F_{ev}$ the spallation shell "1" isn't geometrically closed (this is the right cupola in Figure 1B) [2, 13, 14].

Figure 3 presents results of long (up to 0.2 μs) simulation done by the 2T-HD code. Long duration of the run allows to achieve the stage when pressure at the contact drops to (i) saturation pressure of gold and later to (ii) critical pressure of water. The last instant is marked by the black circle in Figure 3B. After that instant the bubble in water begins to form. Equation of state for water was taken from the database [16].

Integrating along trajectory shown in Figure 3B we find the resulting gain of an amplitude of contact perturbation shown in Figure 3C. Increasing of amplitude of linear perturbation with wavelength λ along the contact continues up to the moment when surface tension cutting of increment at wavelength $\lambda_\sigma(t)$ achieves the considered wavelength λ. We see that significant amplification takes place.

Results of molecular dynamics simulation are shown in Figure 4. Large scale simulation is based on our own interatomic potentials for gold and water. Simulation confirms details found in 2T-HD runs: wide cavitation zone, formation of atmosphere, accretion of foam onto atmosphere, RT instability of contact. MD gives pictures of non-linear growth of RTI. It shows scale enlargement typical for RTI and decay of jets into droplets. Decay of deceleration, surface tension and viscosity play important roles.

We consider different aspects of foaming of molten metal under action of intense ultrashort laser action. Dynamics of expansion of cavitation zone in case of large fluences few times above ablation threshold is analyzed in Section 2. This foam plays definitive role in gold-water dynamic interaction. 1D structure of gold-water flow is studied in Sections 2. It is found that atmosphere like layer from gold forms at contact with water.

The atmosphere from one side is decelerated by water, while from another side it is attacked by fragments of foam falling to atmosphere. This mass and momentum flux decreases deceleration of atmosphere. Linear stability analysis based on 1D trajectory of contact from 1D 2T-HD simulations points out to limited growth of RT perturbations. Direct MD simulation allows to understand non-linear details of development of instability.

ACKNOWLEDGMENTS

This research was support by Russian Science Foundation (RSCF) project No. 14-19-01599.

REFERENCES

[1] J.Xiao, P. Liu, C. X. WangG, G. W. Yang Progress in Materials Science **87,** pp. 140-220 (2017)

[2] N.A. Inogamov, V.V. Zhakhovskii, S.I. Ashitkov, Yu.V. Petrov, M.B. Agranat, S.I. Anisimov, K. Nishihara, and V.E. Fortov, J. Experim. Theor. Phys. (JETP) **107,** No. 1, pp. 1-19 (2008)

[3] G.E. Norman, S.V. Starikov, and V.V. Stegailov, J. Experim. Theor. Phys. (JETP) **114,** No. 5, pp. 792-800 (2012)

[4] N.A. Inogamov, V.V. Zhakhovskii, and V.A. Khokhlov, J. Experim. Theor. Phys. (JETP) **120,** No. 1, pp. 15-48 (2015)

[5] S.I. Ashitkov, P.S. Komarov, V.V. Zhakhovsky, Yu.V. Petrov, V.A. Khokhlov, A.A. Yurkevich, D.K. Ilnitsky, N.A. Inogamov, and M.B. Agranat, J. Phys.: Conf. Ser. **774,** No. 1, 012097 (2016)

[6] R. Fang, A. Vorobyev, and C. Guo, Light: Sci. Appl. **6,** No. 3, e16256 (2017)

[7] N.A. Inogamov, V.V. Zhakhovsky, S.I. Ashitkov, Yu.N. Emirov, A.Ya. Faenov, Yu.V. Petrov, V.A. Khokhlov, M. Ishino, B.J. Demaske, M. Tanaka, N. Hasegawa, M. Nishikino, S. Tamotsu, T.A. Pikuz, I.Y. Skobelev, T. Ohba, T. Kaihori, Y. Ochi, T. Imazono, Y. Fukuda, M. Kando, Y. Kato, T. Kawachi, S.I. Anisimov, M.B. Agranat, I.I. Oleynik, V.E. Fortov, Engineering Failure Analysis **47,** pp. 328-337 (2015)

[8] E.L. Gurevich, Phys. Rev. E **83,** 031604 (2011)

[9] S.I. Ashitkov, S.A. Romashevskii, P.S. Komarov, A.A. Burmistrov, V.V. Zhakhovskii, N.A. Inogamov, and M.B. Agranat, Quantum Electronics **45,** No. 6, pp. 547-550 (2015)

[10] N.A. Inogamov, V.V. Zhakhovsky, V.A. Khokhlov, S.I. Ashitkov, Yu.N. Emirov, K.V. Khichshenko, A.Ya. Faenov, T.A. Pikuz, M. Ishino, M. Kando, N. Hasegawa, M. Nishikino, P.S. Komarov, B.J. Demaske, M.B. Agranat, S.I. Anisimov, T. Kawachi, and I.I. Oleynik, J. Phys.: Conf. Ser. **510,** 012041 (2014)

[11] S.I. Ashitkov, N.A. Inogamov, V.V. Zhakhovsky, Yu.N. Emirov, M.B. Agranat, I.I. Oleinik, S.I. Anisimov, and V.E. Fortov, JETP Lett. **95,** No. 4, pp. 176-181 (2012)

[12] C. Wu, M.S. Christensen, J.-M. Savolainen, P. Balling, and L.V. Zhigilei, Phys. Rev. B **91,** 035413 (2015)

[13] M.B. Agranat, S.I. Anisimov, S.I. Ashitkov, V.V. Zhakhovskii, N.A. Inogamov, K. Nishihara, A.M. Oparin, Yu.V. Petrov, V.E. Fortov, V.A. Khokhlov, Appl. Surf. Sci. **253,** No. 15, pp. 6276-6282 (2007)

[14] Chengping Wu and L.V. Zhigilei, Appl. Phys. A **114,** pp. 11-32 (2014)

[15] L.V. Zhigilei, Zhibin Lin, and D.S. Ivanov, J. Phys. Chem. C **113,** pp. 11892-11906 (2009)

[16] http://teos.ficp.ac.ru/rusbank/